Published in final edited form as:
Matrix Biol. 2004 November ; 23(7): 421–432. doi:10.1016/j.matbio.2004.09.007.

Homozygous ablation of fibroblast growth factor-23 results in hyperphosphatemia and impaired skeletogenesis, and reverses hypophosphatemia in *Phex*-deficient mice

Despina Sitara[a], **Mohammed S. Razzaque**[a], **Martina Hesse**[b], **Subbiah Yoganathan**[c], **Takashi Taguchi**[d], **Reinhold G. Erben**[b], **Harald Jüppner**[e], and **Beate Lanske**[a,*]

[a]Department of Oral and Developmental Biology, The Forsyth Institute, Harvard School of Dental Medicine, 140 The Fenway, Boston, MA, 02115, USA

[b]Institute of Physiology, Physiological Chemistry and Animal Nutrition, Ludwig Maximilians University, Munich, Germany

[c]Animal Facility, The Forsyth Institute, Boston, MA, USA

[d]Department of Pathology, Nagasaki University, Graduate School of Medical Sciences, Nagasaki, Japan

[e]Endocrine Unit, Massachusetts General Hospital and Harvard Medical School, Boston, MA, USA

Abstract

Fibroblast growth factor-23 (FGF-23), a recently identified molecule that is mutated in patients with autosomal dominant hypophosphatemic rickets (ADHR), appears to be involved in the regulation of phosphate homeostasis. Although increased levels of circulating FGF-23 were detected in patients with different phosphate-wasting disorders such as oncogenic osteomalacia (OOM) and X-linked hypophosphatemia (XLH), it is not yet clear whether FGF-23 is directly responsible for the abnormal regulation of mineral ion homeostasis and consequently bone development. To address some of these unresolved questions, we generated a mouse model, in which the entire *Fgf-23* gene was replaced with the *lacZ* gene. *Fgf-23* null (*Fgf-23*$^{-/-}$) mice showed signs of growth retardation by day 17, developed severe hyperphosphatemia with elevated serum 1,25$(OH)_2D_3$ levels, and died by 13 weeks of age. Hyperphosphatemia in *Fgf-23*$^{-/-}$ mice was accompanied by skeletal abnormalities, as demonstrated by histological, molecular, and various other morphometric analyses. *Fgf-23*$^{-/-}$ mice had increased total-body bone mineral content (BMC) but decreased bone mineral density (BMD) of the limbs. Overall, *Fgf-23*$^{-/-}$ mice exhibited increased mineralization, but also accumulation of unmineralized osteoid leading to marked limb deformities. Moreover, *Fgf-23*$^{-/-}$ mice showed excessive mineralization in soft tissues, including heart and kidney. To further expand our understanding regarding the role of *Fgf-23* in phosphate homeostasis and skeletal mineralization, we crossed *Fgf-23*$^{-/-}$ animals with *Hyp* mice, the murine equivalent of XLH. Interestingly, *Hyp* males lacking both *Fgf-23* alleles were indistinguishable from *Fgf-23*$^{-/-}$ mice, both in terms of serum phosphate levels and skeletal changes, suggesting that *Fgf-23* is upstream of the phosphate regulating gene with homologies to endopeptidases on the X chromosome (Phex) and that the increased plasma Fgf-23 levels in *Hyp* mice (and in XLH patients) may be at least partially responsible for the phosphate imbalance in this disorder.

*Corresponding author. Tel.: +1 617 432 5748; fax: +1 617 432 5767. .

Keywords

Fgf-23 null; *Hyp*; Phosphate; Mineralization; Bone

1. Introduction

Inorganic phosphate (Pi) is not only essential for intracellular signalling, DNA synthesis, and energy metabolism, but it is also essential for normal skeletal growth and development. However, despite its broad biological importance, the regulation of phosphate homeostasis is not clearly understood. Recent advances have provided new insights into the complex mechanisms involved in renal phosphate handling and bone mineralization (Drezner, 2002). Particularly the molecular definition of two phosphate-wasting disorders, X-linked hypophosphatemia (XLH), which is caused by mutations in PHEX (Holm et al., 1997; HYP_Consortium, 1995), and autosomal dominant hypophosphatemic rickets (ADHR), which is caused by mutations in FGF-23 (ADHR_Consortium, 2000; Econs et al., 1997; White et al., 2001), has identified important factors involved in the regulation of phosphate homeostasis. Furthermore, overexpression of FGF-23 was found in some tumors that cause oncogenic osteomalacia (OOM) (Seufert et al., 2001; Shimada et al., 2001; White et al., 2002); a significant elevation of plasma FGF-23 concentrations was detected in these patients (Jonsson et al., 2003; Nelson et al., 2003; Yamazaki et al., 2002). Several phosphaturic factors, including FGF-23, frizzled-related protein 4 (FRP4), and matrix extracellular phosphoglycoprotein (MEPE) were cloned from cDNA libraries derived from OOM tumors (Berndt et al., 2003; De Beur et al., 2002; Rowe et al., 2004; Shimada et al., 2001), for instance, hemangiopericytoma.

Understanding the molecular and cellular mechanisms involved in the regulation of phosphate homeostasis is particularly important as low serum phosphate levels can result in defective skeletal growth and mineral ion deposition, in turn leading to osteomalacia and rickets. In contrast, high serum phosphate levels contribute to the development of arteriosclerosis, soft tissue calcifications in mice and human, and secondary hyperparathyroidism, particularly in end-stage renal disease in human (Bai et al., 2002; Dunstan et al., 2004; Imanishi et al., 2004; Larsson et al., 2003; Schiavi and Kumar, 2004; Weber et al., 2003).

Recently, recombinant FGF-23 was shown to selectively enhance renal phosphate excretion when given in vivo (Shimada et al., 2004a; Shimada et al., 2002). Furthermore, transgenic mice overexpressing human wild-type FGF-23 under the control of different promoters showed hypophosphatemia and increased urinary phosphate excretion due to reduced expression of the sodium-dependent phosphate cotransporter types IIa (NaPi-2a) and IIc (NaPi-2c) in the renal cortex (Larsson et al., 2004; Shimada et al., 2004b). Renal phosphate wasting in these transgenic mice also led to skeletal abnormalities such as disrupted growth plates and reduced bone mineral density (BMD) (Larsson et al., 2004; Shimada et al., 2004b). Similarly, transgenic mice overexpressing human (R176Q) FGF-23, a mutant form of FGF-23 resistant to degradation by furin-like proteases (Bai et al., 2003), showed more pronounced hypophosphatemia and rickets/osteomalacia (Bai et al., 2004) than animals expressing the wild-type FGF-23 (Bai et al., 2003; Saito et al., 2003).

XLH is the most common form of inherited rickets, which is caused by inactivating mutations in a phosphate-regulating gene with homologies to endopeptidases on the X-chromosome, termed *PHEX* (HYP_Consortium, 1995). *Hyp* mice represent the murine homologue of XLH (Du et al., 1996; Strom et al., 1997; Tenenhouse, 1999), and these animals exhibit renal phosphate wasting and hypophosphatemia, as well as high serum Fgf-23 levels (Aono et al., 2003). On the other hand, targeted disruption of *Fgf-23* gene in mice was shown to result in hyper-phosphatemia, diminished phosphate excretion, and up-regulation of NaPi-2a

expression in proximal tubular cells as well as decreased bone mineral density (Shimada et al., 2004a).

Despite recent advances in our understanding of FGF-23 in the regulation of phosphate homeostasis and bone development, several key questions remain to be solved. For instance, the cellular source of FGF-23 and effector organs are not yet clearly defined (Carpenter, 2003; Riminucci et al., 2003; Strewler, 2001).

Furthermore, reported studies provide conflicting data regarding the role of PHEX in the degradation of FGF-23 (Bowe et al., 2001; Campos et al., 2003; Liu et al., 2003), and it remains uncertain whether FGF-23 is responsible for phosphate wasting in patients with XLH or in *Hyp* mice. To address some of these partially resolved questions, we generated *Fgf-23* null mice by replacing the entire coding region (exons 1-3) of the mouse *Fgf-23* gene with the *lacZ* gene, thus providing a sensitive tool for examining the expression pattern of *Fgf-23* during embryonic and post-embryonic development.

2. Results

2.1. Generation of Fgf-23 null mice

Targeted deletion of the *Fgf-23* gene resulted in viable heterozygous (*Fgf-23*$^{+/-}$) and homozygous mutant animals (*Fgf-23*$^{-/-}$) (Fig. 1A and B). Heterozygous mice appeared to be healthy and were fertile. *Fgf-23*$^{-/-}$ mice were born at the expected Mendelian ratio, and, at birth, their gross appearance were indistinguishable from those of their wild-type littermates. The number of males and females born was comparable (30 females vs. 28 males). By day 10, *Fgf-23* null animals showed visually detectable growth retardation, which became significantly different by day 17. The mean body weight of *Fgf-23*$^{-/-}$ mice at 11 weeks was 6.6±0.2 vs. 23.6 ±1.1 g for *Fgf-23*$^{-/-}$ and wild-type males, respectively ($p<0.001$). Moreover, the longevity of the *Fgf-23*$^{-/-}$ mice was markedly shorter than that of either wild-type or heterozygous *Fgf-23*$^{+/-}$ littermates. The survival rate of homozygous mice did not differ significantly between male and female ($p=0.6965$); all *Fgf-23*$^{-/-}$ animals had died by 13 weeks of age.

2.2. Expression of lacZ under the control of the endogenous Fgf-23 promoter

To study *Fgf-23* expression prenatally, we performed β-galactosidase staining of heterozygous and wild-type embryos at E11.5 (data not shown) and E12.5. LacZ-positive staining was clearly detectable in three predominant sites: heart, liver, and somites; wild-type littermates did not show any staining (Fig. 1C). To evaluate the expression of *Fgf-23* postnatally, we performed lacZ staining using skull bones, such as calvaria, obtained from 4- and 6-week-old wild-type and *Fgf-23*$^{-/-}$ mice. Strong blue staining was visible in osteoblasts and cells at the sutures of mutants; no lacZ staining was detected in bones of wild-type controls, even after an extended period of staining.

2.3. Serum measurements in Fgf-23$^{-/-}$ mice

Serum phosphate levels of wild-type and *Fgf-23*$^{-/-}$ male and female mice were assessed at 3 and 6 weeks. *Fgf-23*$^{-/-}$ mice ($n=7$) showed significantly higher serum phosphate levels than control littermates ($n=15$; 16.3±0.3 vs. 9.6±0.5 mg/dl) at 3 weeks (see Fig. 7B). In addition, we detected significantly higher serum $1,25(OH)_2D_3$ concentration in *Fgf-23*$^{-/-}$ animals (368.1 ±226.3 pg/ml) than in wild-type mice (56.4±13.8 pg/ml). Similarly, alkaline phosphatase activity was higher in *Fgf-23*$^{-/-}$ than in wild-type mice (990.86±317.22 vs. 238.33±38.45 U/l). There was no significant change in PTH concentration, both in wild-type and mutant mice (data not shown).

2.4. Abnormal bone mineral content and density in Fgf-23$^{-/-}$ mice

Fgf-23$^{-/-}$ mice were markedly growth-retarded and exhibited reduced body weight, size, and consequently skeletal size. We analysed *Fgf-23*$^{-/-}$ and wild-type littermates by dual-energy X-ray absorptiometry (DEXA) for whole-body bone mineral content (BMC) normalized to body weight at 3 (control n=8, *Fgf-23*$^{-/-}$ n=6), 6 (control n=9, *Fgf-23*$^{-/-}$ n=6), and 11 weeks (control n=2, *Fgf-23*$^{-/-}$ n=2). We observed that *Fgf-23*$^{-/-}$ mice had significantly higher BMC/g at all time points measured (Fig. 2A). Furthermore, the difference in BMC/g calculated among *Fgf-23*$^{-/-}$ animals differed significantly at 3, 6, and 11 weeks of age. However, autoradiographic studies (Fig. 2B) showed that the bone mineral density (BMD) of hindlimbs (and forelimbs, data not shown) was strikingly decreased in *Fgf-23*$^{-/-}$ animals. To further validate this observation, we performed additional measurements of fore- and hindlimbs by DEXA. These analyses confirmed that hindlimb BMD of *Fgf-23*$^{-/-}$ animals was significantly reduced at all investigated time points (Fig. 2C). The difference in BMD among *Fgf-23*$^{-/-}$ animals increased significantly with time. We extended our measurements by peripheral quantitative computerized tomography (pQCT) and again found that volumetric BMD of the femoral shaft and the femoral metaphysis was lower in *Fgf-23*$^{-/-}$ (n=7) mice compared with wild-type littermates (n=7) at 4 weeks of age (Fig. 2D).

2.5. Abnormal bone formation, skeletal mineralization, and development of soft tissue calcifications in Fgf-23$^{-/-}$ mutants

To further examine bone mineralization in *Fgf-23*$^{-/-}$ animals, we performed Alizarin Red S staining of wholebody skeletons and compared them with wild-type littermates at 3 and 6 weeks. During dissections, it became evident that *Fgf-23*$^{-/-}$ mice suffered from severe axial and appendicular skeletal malformations, which were confirmed by staining for bone mineral (Fig. 3A). Furthermore, we noted the presence of bone nodules at most ribs and paws and the presence of lesions that were reminiscent of rachitic changes, such as widened epiphysis (ribs) and transparency of stained bones (paw). Excessive mineral accumulation was also noted in areas surrounding the shaft of radius and ulna of *Fgf-23*$^{-/-}$ mice. However, despite increased yet disproportionate accumulation of bone mineral, the mutant bones were abnormally fragile and deformed. Von Kossa staining of different soft tissues at various time points postnatally showed considerable mineralization in non-skeletal tissues of *Fgf-23*$^{-/-}$ mice. As shown in Fig. 3B, abnormal mineralization was detected in various organs, including heart and kidney of older animals.

To further study the mineralization patterns of mutant bones, we performed histological analyses on methylmethacrylate sections (Fig. 4). Histological examination of femurs from 4-week-old *Fgf-23*$^{-/-}$ mice revealed increased osteoid formation in cortical bone. In addition, the growth plates were narrowed with decreased numbers of hypertrophic chondrocytes in the mutants. More mineral deposition was apparent in the primary spongiosa immediately adjacent to the hypertrophic chondrocytes. Histology of ribs and vertebra showed a marked increase in woven bone formation and a striking accumulation of osteoid.

2.6. Chondrocyte and osteoblast differentiation in Fgf-23$^{-/-}$ mice

To further analyse the differentiation status of bone cells, we performed in situ hybridizations on paraffin sections from tibia of *Fgf-23*$^{-/-}$ mice (n=6) and wild-type littermates (n=6) at 3 weeks of age (Fig. 5). We were able to confirm the previously noted (Shimada et al., 2004a) reduction of hypertrophic chondrocytes from 6–10 cell layers in wild-type to 3–5 cell layers in mutant animals, as demonstrated by the marked decrease in collagen type X expression. We also examined expression of osteopontin, a marker of late hypertrophic chondrocytes and early osteoblasts, and observed a relative increase in expression in osteoblasts from *Fgf-23*$^{-/-}$ mice. In contrast, expression of bone gla protein, a marker for mature osteoblasts, was clearly reduced in *Fgf-23*$^{-/-}$ mice.

2.7. Generation and analyses of male Hyp mice lacking both Fgf-23 alleles

To analyse the consequences of complete ablation of both *Fgf-23* and *Phex*, we generated male *Hyp* mice that were null for *Fgf-23* (*Hyp/Fgf-23*$^{-/-}$) and compared the findings to male animals of the genotypes *Hyp/Fgf-23*$^{+/-}$ and *Fgf-23*$^{-/-}$; analyses were performed at 3 weeks of age. Compound mutants (*Hyp/Fgf-23*$^{-/-}$) were viable and indistinguishable from wild-type animals at birth. Gross appearances among the three analysed genotypes are shown in Fig. 6A. Evaluation of bones by X-ray studies (Fig. 6B) showed that *Hyp/Fgf-23*$^{+/-}$ animals exhibited extremely short and thickened femurs, as well as cupping of the metaphysis below the growth plates, findings which are characteristic of *Hyp* mice (Miao et al., 2001). In comparison, bones of compound mutants were longer and thinner with relatively regular appearing growth plates. We further analysed the mineralization pattern of the skeleton of these animals by Alizarin Red S staining (Fig. 7A) at 3 weeks of age. In contrast to *Hyp/Fgf-23*$^{+/-}$ animals, which did not show any apparent changes compared to wild-type males (see Fig. 3A), the skeleton of the compound mutants *Hyp/Fgf-23*$^{-/-}$ resembled more closely that of *Fgf-23*$^{-/-}$ mice. In particular, *Hyp/Fgf-23*$^{-/-}$ animals showed similar nodular deformities in ribs and paws that were initially observed in *Fgf-23*$^{-/-}$ mice (Fig. 7A, shown by arrows). Histological analyses on methylmethacrylate sections of femurs from 3-week-old mice showed strong resemblance in the mineralization pattern of *Hyp/Fgf-23*$^{-/-}$ and *Fgf-23*$^{-/-}$ mice. Serum phosphate level was significantly higher in *Hyp/Fgf-23*$^{-/-}$ animals (14.2±1.6 mg/dl, n=2) than in *Hyp* mice (about 4 mg/dl), as previously reported (Lorenz-Depiereux et al., 2004), and thus were similar to those observed in *Fgf-23*$^{-/-}$ mice (16.3±0.28) (Fig. 7B;Shimada et al., 2004a).

3. Discussion

In the present study, we generated mice in which the entire coding region of the *Fgf-23* gene had been replaced with the *lacZ* gene and the *neomycin*-resistance cassette. In comparison to wild-type littermates, mice with ablation of both *Fgf-23* alleles were smaller in size, showed gross deformities of numerous skeletal elements, and died prematurely. These animals furthermore had severe hyper-phosphatemia and elevated serum $1,25(OH)_2D_3$ levels, which confirms that Fgf-23 is an important regulator of 1-alpha hydroxylase activity (Larsson et al., 2004; Shimada et al., 2004a) In contrast, heterozygous *Fgf-23*$^{-/+}$ animals showed no obvious skeletal abnormalities, and their size and longevity were similar to those of wild-type littermates, suggesting that *Fgf-23* haploinsufficiency does not lead to obvious consequences. Since our findings were indistinguishable from those recently described for mice homozygous for ablation of *Fgf-23* exon 1 alone (Shimada et al., 2004a), the replacement of *Fgf-23* with the *lacZ* reporter, as in the animals described in this report, does not appear to affect the phenotype of *Fgf-23*$^{-/-}$ mice.

Earlier studies have shown that treatment of wild-type mice with recombinant intact human FGF-23 increases urinary phosphate excretion leading to hypophosphatemia (Shimada et al., 2001). Furthermore, the transgenic expression of wild-type or mutant FGF-23 resulted in severe rickets/osteomalacia (Bai et al., 2004; Larsson et al., 2004; Shimada et al., 2004b), but it remained uncertain whether these changes were due to direct effects of Fgf-23 on cartilage and bone or were simply related to changes in phosphate homeostasis. *FGF-23* is expressed in normal bone-forming osteoblasts and their progenitors, with a particularly prominent increase of its mRNA at sites of new bone formation due to fractures (Riminucci et al., 2003). This makes it plausible that Fgf-23 is directly involved in normal bone formation. In accord with the notion, our *Fgf-23* null animals displayed considerable reductions in BMD. Similar observations had also been documented and reported earlier (Shimada et al., 2004a). It thus appears likely that Fgf-23, locally produced in bone cells, affects through paracrine/autocrine mechanisms the regulation of bone formation, while the observed mineralization defect may

be caused, at least partially, by changes in phosphate homeostasis and/or increased 1,25 $(OH)_2D_3$ levels.

Lack of *Fgf-23*, however, led to exostotic changes at several sites, e.g., ribs and phalanges (see Fig. 3A). This makes it plausible that this novel growth factor also has an important role in preventing bone formation at certain skeletal sites (see also below). *Fgf-23* null mice furthermore showed a decreased zone of hypertrophic chondrocytes, making it likely that Fgf-23 has a role in chondrocyte growth and differentiation, unless the observed changes are secondary to the abnormalities in serum phosphate and/or $1,25(OH)_2D_3$ concentration or to other changes that involve PTHrP-dependent signalling through the PTH/PTHrP receptor (Kronenberg, 2003). In addition, *Fgf-23* may contribute to regulating the expression of other molecules, such as *PHEX* (HYP_Consortium, 1995), *MEPE* (Argiro et al., 2001;Quarles, 2003;Rowe et al., 2004), *LRP-5/Wnt*, and/or *FRP4* (Schiavi and Kumar, 2004).

Fgf-23 is expressed only at low levels in certain tissues and organs, including brain, bone, heart, and thymus (Liu et al., 2003; Riminucci et al., 2003; Shimada et al., 2001; Yamashita et al., 2000). The presence of *lacZ* as a marker for *Fgf-23* expression therefore provided a useful marker for assessing its expression pattern during embryonic and postembryonic development of *Fgf-23*$^{+/-}$ mice, i.e., animals with presumably undisturbed phosphate homeostasis. The expression pattern of *Fgf-23* in embryonic tissues has not yet been studied in any detail, while some studies have reported very weak expression of *FGF-23* transcripts in adult liver, lymph node, thymus, heart, and brain (Liu et al., 2003; Shimada et al., 2001; Yamashita et al., 2000). The presence of the *lacZ* gene may furthermore allow a rapid detection of changes in *Fgf-23* expression induced by phosphate, $1,25(OH)_2D_3$, and other factors, and it may help with the identification and isolation of *Fgf-23*$^{+/-}$ cells, which could be useful in studying the regulation of Fgf-23 synthesis and secretion in vitro. Our *Fgf-23*$^{+/-}$ mice with knock-in of the *lacZ* gene will therefore be of particular significance for further exploring the cells producing Fgf-23 and studying the molecules that regulate its synthesis and secretion.

Hyp mice, the murine equivalent of XLH patients, show renal phosphate wasting leading to hypophosphatemia and thus impaired skeletal mineralization (Xiao et al., 1998). In these animals, Fgf-23 levels were shown to be elevated (Aono et al., 2003), which is similar to the findings in patients with XLH (Jonsson et al., 2003; Shimada et al., 2002; Weber et al., 2003). Using our *Fgf-23*$^{-/-}$ mice, we were able to modify the hypophosphatemia and rickets in *Hyp* mice. In fact, serum phosphate levels were reversed in the compound *Hyp/Fgf-23*$^{-/-}$ mice. This could indicate that Phex/PHEX is either directly or indirectly involved in the degradation of intact biologically active *FGF-23*. However, in vitro studies have thus far provided no consistent results regarding the role of Phex/PHEX in this process; only one reported study suggested PHEX-dependent degradation of wild-type FGF-23 (Bowe et al., 2001) but not of FGF-23 with the R176Q mutation (Bai et al., 2003; Liu et al., 2003). Our compound *Hyp/Fgf-23*$^{-/-}$ mice showed biochemical and morphological features that are similar to those we found in *Fgf-23*$^{-/-}$ knockout mice. Indeed, in contrast to the hypophosphatemia observed in *Hyp* mice (Lorenz-Depiereux et al., 2004), *Hyp/Fgf-23*$^{-/-}$ males showed serum phosphate levels that were indistinguishable from those of *Fgf-23*$^{-/-}$ animals. This suggests that Fgf-23 resides upstream of Phex, although it does not provide enough information for a direct role of this endopeptidase in the degradation of Fgf-23. The “rescued” *Hyp* mice furthermore showed exostosis-like skeletal changes at ribs and digits, emphasizing the fact that Fgf-23 is not only involved in bone formation but may also have additional roles in preventing bone formation at aberrant sites.

One of the significant findings of this study was extensive soft tissue mineralization in *Fgf-23*$^{-/-}$ mice. This is of particular importance because high serum phosphate levels could contribute to the development of arteriosclerosis and other soft tissue calcifications and could

lead to secondary hyperparathyroidism; these are major complications encountered in end-stage renal disease patients undergoing haemodialysis. The cardiovascular mortality rate is 20 to 40 times higher for adults on dialysis than for the general population (Collins et al., 2001). Recent studies documented hyperphosphatemia and increased calcium phosphate product as contributing factors to increased mortality in dialysis patients (Block et al., 1998; Block and Port, 2000; Ganesh et al., 2001). Although accelerated coronary calcification in end-stage renal disease patients is thought to be related to inadequate or inappropriate treatment of hyperphosphatemia, our lack of understanding of phosphate homeostasis makes it difficult to develop any long-term therapeutic strategies. Commonly used phosphate binders to minimize hyperphosphatemia contain aluminum or calcium. Aluminum accumulates in the tissues and causes neurologic, skeletal, and haematologic toxicities (Alfrey et al., 1976; Ott et al., 1982), while ingestion of calcium carbonate, an effective phosphate binder, leads to hypercalcemia and increases the risk of vascular calcification in end-stage renal disease patients (Meric et al., 1990; Slatopolsky et al., 1986). Recently, a novel calcium- and aluminum-free phosphate binder, poly(allylamine hydrochloride) (RenaGel), was reported to reduce serum phosphorus and iPTH concentrations without significant changes in serum calcium levels (Chertow et al., 1997; Slatopolsky et al., 1999); it will be interesting to determine whether the phosphate-lowering effects of this newly developed agent exert its effect through manipulating FGF-23.

In summary, we have generated *Fgf-23* knockout animals, which showed hyperphosphatemia, increased levels of $1,25(OH)_2D_3$, and numerous skeletal abnormalities, which reversed the development of hypophosphatemia in *Hyp* mice. These animals will facilitate further exploration of Fgf-23 biology. Since *Fgf-23* was replaced with the *lacZ* reporter, our mice will also provide an additional in vivo tool to determine the role of Fgf-23 during early development and will facilitate designing in vitro studies to examine the transcriptional activation, synthesis, and secretion of Fgf-23.

4. Experimental procedures

4.1. Generation of Fgf-23 null animals

Using the cDNA encoding mouse *Fgf-23*, kindly provided by Dr. Tim Strom, Gesellschaft für Umwelt und Gesund-heitsforschung, Munich, Germany, a Sv129J mouse genomic library in lambda Dash II (kindly provided by T. Doetschmann) was screened. Three clones (clones 24, 25, and 27) were identified containing the full-length gene and additional 15 kb of 5′ and 3′ flanking sequences. For construction of the targeting vector, the entire coding region (exons 1–3) of the mouse *Fgf-23* gene was replaced with the *lacZ* gene and the *neomycin* (*neo*) resistance gene. The coding region of the *lacZ* gene was cloned—in frame—downstream of the initiator methionine of *Fgf-23* such that lacZ translation will start at the translational start site for *Fgf-23*.

The pPNT plasmid was used as a backbone to construct the targeting vector (Bradley, 1987). A ~5-kb *Eco*RI-*Bam*HI fragment derived from the 5′ noncoding region of *Fgf-23* was chosen as the 5′ flanking region. After cutting with *Eco*RI and blunt-ending, the *Eco*RI–*Bam*HI fragment was released from the genomic DNA clone with *Bam*HI. This fragment was then cloned into the *Bam*HI site and the blunt-ended *Xba*I site of the vector carrying the *lacZ* gene (pβGal); the restriction sites for *Eco*RI in the fragment of the mouse gene and the *Xba*I site in the vector are thus no longer present. A "*Bam*HI connector" carrying the initiator methionine was cloned into the preserved *Bam*HI site to connect the 3′ end of the 5′ flanking region of *Fgf-23* to the *lacZ* gene. The combined fragment was then released by digestion with *Not*I/*Xho*I and cloned into *Not*I/*Xho*I sites of the pPNT targeting vector, immediately upstream of the *neo* cassette. A 4-kb *Xho*I–*Eco*RI fragment derived from the 3′ end of the *Fgf-23* gene was made blunt by Klenow enzyme and was then cloned immediately downstream of the *neo* gene by ligation into blunt-ended *Eco*RI sites of the vector to generate the final targeting vector,

pPNT-Fgf-23; 5′ and the 3′ nucleotide sequences and orientation of each DNA fragment were confirmed by sequence analysis. Since the pPNT-*Fgf-23* vector contains also the herpes simplex virus thymidine kinase (HSV-tk) gene flanked by the PGK-1 promoter and polyadenylation signal, the vector is thus designed to allow double selection for homologous recombination events prior to screening by Southern blot analysis (Karaplis et al., 1994). The *pPNT-Fgf-23* was linearized using the restriction enzyme *Not*I and electroporated into ES cells. After double selection of ES cells for the presence of the *neo* gene with G418 (300 μg/ml), and for absence of the HSV-Tk gene with FIAU (0.2 μM), 192 surviving ES cell clones were isolated and expanded, and 27 (14%) were shown by Southern blot analyses to have undergone homologous recombination (data not shown). Two independent ES cell clones resulted in germline transmission. Mice were fed standard diet (7012 Harlan Teklad LM-485 autoclavable rodent diet), containing 0.62% phosphorus and 0.84% calcium, and autoclaved tap water. All animal experiments were approved by the institutional care and use committee at the Forsyth Institute (Harvard School of Dental Medicine).

4.2. Southern blot and PCR analyses

Genotyping was performed initially by Southern blot analysis. Genomic DNA (~10 μg) purified from tail clips using standard procedures was digested with *Bgl*II and hybridized to an external probe (Probe A 367 bp) (Fig. 1). The expected lengths of the *Bgl*II fragments were 17 kb for the wild-type allele and 10 kb for the mutant allele (Fig. 1A, B). Further genotyping of mice was performed by PCR using the following specific primers: *Fgf-23* forward 5′-AGT GGA CGC TGG AGA ATG GCT ATG-3′, *Fgf-23* reverse 5′-CTG GGA AAG GGG CGA CAC C-3′; *Neo* forward 5′-GAT CGG CCA TTG AAC AAG ATG-3′, *Neo* reverse 5′-AAG GTG AGA TGA CAG GAG ATC-3′. After an initial denaturation for 5 min at 94 °C, amplification cycles consisted of denaturation at 94 °C for 1 min, annealing at 58 °C for *Neo* and 65 °C for *Fgf-23* for 1 min, and 1-min extension at 72 °C for 35 cycles followed by a final extension for 10 min at 72 °C. The expected product size for *Fgf-23* is 397 bp and, for *Neo*, 310 bp.

4.3. LacZ staining

Fgf-23 mRNA expression was achieved through μ-galactosidase staining of *Fgf-23*$^{+/-}$ embryos at E12.5 and calvaria of *Fgf-23*$^{-/-}$ animals at 3 and 6 weeks. Tissues were fixed in a mixture of 37% formaldehyde and 25% glutaraldehyde on ice for a maximum of 2 h followed by three washes (15 min each) in a rinse buffer containing 0.02% NP-40 (Roche)/PBS at room temperature. Subsequently, tissues were stained at 37 °C for 30 min (calvaria) and overnight (embryos) in a shaker placed in a dark incubator. Staining solution contained 5mM $K_3Fe(CN)_6$ (ACROS Organics), 5mM $K_4Fe(CN)_6$ (ICN Biomedicals), 0.01% DCA, 2mM $MgCl_2$, 0.02% NP-40, 5mM EGTA, and 1 mg/ml X-gal (TAKARA), in 1× PBS.

4.4. PIXImus and quantitative computerized tomography (pQCT)

Bone mineral density (BMD) and bone mineral content (BMC) were determined on 3-, 6-, and 11-week-old wild-type and *Fgf-23* null animals. Mice were anaesthetized by intraperitoneal injection with ketamine and xylazine (0.087 mg of ketamine and 0.013 mg of xylazine per 1 g of body weight). Measurements were determined using the PIXImus small animal dual-energy X-ray absorptiometry (DEXA) system (Lunar), with data analysis of software version 1.4x. Bone mineral density is a two-dimensional measurement comprised of mineral within the area determined to be bone by the present thresholds in the PIXImus densitometer. The resolution of the PIXImus is 0.8×0.18-mm pixels with a usable scanning field of 80×100 mm, allowing for measurement of single whole mice and collection of isolated specimens. Calibrations were performed with a phantom of known density, and quality assurance measurements were performed prior to BMD measurements.

BMD of the left femur was measured by peripheral quantitative computerized tomography (pQCT) using a XCT Research M+pQCT machine (Stratec Medizintechnik, Pforzheim, Germany). The measurements were made with a collimator opening of 0.2 mm on specimens stored in 70% ethanol. One slice in the middiaphysis of the femur, and three slices in the distal femoral metaphysis located 1.5, 2, and 2.5 mm proximal to the articular surface of the knee joint were measured. All BMD values of the distal femoral metaphysis were calculated as the mean over three slices. A voxel size of 0.070 mm and a threshold of 600 mg/cm^3 were used for calculation of cortical BMD.

4.5. X-ray studies

X-rays of mice were taken by the Faxitron MX-20 Specimen Radiography System (Faxitron X-ray, Wheeling, IL) using a Kodak Portal Oncology film (Eastman-Kodak). Measurements were taken at 33 kV with a 30-s exposure. The image was developed by a Kodak M35A X-OMAT processor (Kodak Diagnostic Imaging).

4.6. Skeletal staining with Alizarin Red S

The mineralization pattern of the skeleton was analysed in 3- and 6-week-old mice as described earlier by McLeod (McLeod, 1980). Briefly, adult mice were skinned, eviscerated, and fixed in 95% ethanol. Subsequently, acetone was used to remove fat. Skeletons were then stained by Alizarin Red S and sequentially cleared in 1% potassium hydroxide. Mineralized bones were visualized by red staining.

4.7. Histology and tissue preparation

For histological analyses, paraffin sections of bones and soft tissues were produced at 3 and 11 weeks postnatally. Animals were dissected, and tissues were fixed in 4% paraformaldehyde (PFA)/PBS pH 7.4 at 4 °C for several days. Bones were subsequently demineralized for 1–2 weeks in 20% EDTA. All tissues were rinsed in PBS, dehydrated at room temperature through an ethanol series: 70% for 6 h, 80% for 1 h, 96% for 1 h, and 100% for 3 h, cleared twice in xylene for 1 h/step, embedded in paraffin, serial sectioned at 6 μm using a Microm HM 360 microtome (Microm, Walldorf, Germany), and mounted on SuperFrost Plus slides.

To obtain methylmethacrylate sections, samples were fixed in 4% PFA for 24 h at 4 °C and washed overnight in PBS containing 10% sucrose at 4 °C. Subsequently, bones were dehydrated and embedded undecalcified in methylmethacrylate. Three-micrometer-thick sections were prepared from various sites of the skeleton, including ribs, vertebra, and femurs using a HM 360 microtome (Microm) and stained with von Kossa/toluidine blue (Schenk et al., 1984).

4.8. Riboprobes and in situ hybridization

Complementary ^{35}S-UTP-labeled riboprobes (complementary RNAs for collagen type X, osteopontin, and bone gla protein) were used for performing in situ hybridization on paraffin sections. Plasmids encoding the cDNA were linearized with appropriate restriction enzymes to transcribe either antisense or sense riboprobes in vitro using the appropriate RNA polymerase. In situ hybridization was carried out as described previously (Lanske et al., 1998). Briefly, bone sections were deparaffinized in xylene and rehydrated in a decreasing ethanol series (100%, 90%, 70%). After proteinase K treatment and postfixation in 4% PFA, sections were incubated in 0.2N HCl. Sections were then acetylated with 0.25% acetic anhydride in triethanolamine buffer. Before hybridization was performed, sections were dehydrated in 70% and 95% ethanol and air-dried. Sections were then hybridized with ^{35}S-labeled antisense riboprobes in a humidified chamber at 55 °C for 16 h. After hybridization, nonspecifically bound riboprobes were removed by washing the slides with 2 × SSC and 2×

SSC/50% formamide at 50 °C and treating them with RNase at 37 °C for 20 min. The final wash steps were performed once in 2× SSC and twice in 0.2× SSC at 50 °C for 20 min. To detect the hybridization of riboprobes on tissues, sections were dehydrated in 70% and 95% ethanol and air-dried. To estimate the intensity of bound riboprobes, slides were exposed overnight to X-ray film (Kodak Biomax MR-1) at room temperature. Sections were then coated with Kodak NTB2 emulsion, exposed for the time needed (determined by autoradiography), developed with Kodak Dektol developer, and fixed with Kodak fixer. After counterstaining with hematoxylin and eosin, tissue sections were analysed with a Zeiss microscope using bright- and dark-field optics.

4.9. Measurement of biochemical serum and urinary parameters

Blood was obtained from the vena cava of 3-,4-, and 6-week-old wild-type and *Fgf-23* null animals. Serum was isolated by centrifugation at 3000 ×*g* for 10 min and stored at −80 °C. Serum PTH levels were measured using a Mouse Intact PTH ELISA kit (Immunotopics, San Clemente, CA). Serum concentrations of $1,25(OH)_2D_3$ were measured using a radioreceptor assay (Immundiagnostik, Bensheim, Germany). Serum phosphorus and serum alkaline phosphatase were determined using a Hitachi 766 autoanalyzer (Boehringer Mannheim, Mannheim, Germany).

4.10. Statistical analysis

Statistically significant differences between groups were evaluated by Student's *t* test for comparison between two groups or by one-way analysis of variance (ANOVA) for multiple comparison. All values were expressed as mean-±S.E.M. A *p* value less than 0.05 was considered to be statistically significant. All analyses were performed using Microsoft Excel and GraphPad Prism 3.0.

Acknowledgments

The authors wish to thank C. Carr for her technical help, J. Saxton for performing the histological sections, and Dr. R. Bronson for helpful discussions. This work was supported by a fund provided to BL from Harvard School of Dental Medicine.

References

ADHR_Consortium. Autosomal dominant hypophosphataemic rickets is associated with mutations in FGF23. The ADHR Consortium. Nat. Genet 2000;26:345–348. [PubMed: 11062477]

Alfrey AC, LeGendre GR, Kaehny WD. The dialysis encephalopathy syndrome. Possible aluminum intoxication. N. Engl. J. Med 1976;294:184–188. [PubMed: 1244532]

Aono Y, Shimada T, Yamaziki Y, Hino R, Takeuchi Y, Fujita T, Fukumoto S, Nagano N, Wada M, Yamashita T. The neutralization of FGF-23 ameliorates hypophosphatemia and rickets in Hyp mice. J. Bone Miner. Res 2003;18(Suppl. 2):1056.

Argiro L, Desbarats M, Glorieux FH, Ecarot B. Mepe, the gene encoding a tumor-secreted protein in oncogenic hypophosphatemic osteomalacia, is expressed in bone. Genomics 2001;74:342–351. [PubMed: 11414762]

Bai X, Miao D, Panda D, Grady S, McKee MD, Goltzman D, Karaplis AC. Partial rescue of the Hyp phenotype by osteoblast-targeted PHEX (phosphate-regulating gene with homologies to endopeptidases on the X chromosome) expression. Mol. Endocrinol 2002;16:2913–2925. [PubMed: 12456809]

Bai XY, Miao D, Goltzman D, Karaplis AC. The autosomal dominant hypophosphatemic rickets R176Q mutation in fibroblast growth factor 23 resists proteolytic cleavage and enhances in vivo biological potency. J. Biol. Chem 2003;278:9843–9849. [PubMed: 12519781]

Bai X, Miao D, Li J, Goltzman D, Karaplis AC. Transgenic mice overexpressing human fibroblast growth factor 23(R176Q) delineate a putative role for parathyroid hormone in renal phosphate wasting disorders. Endocrinology 2004;145:5269–5279. [PubMed: 15284207]

Berndt T, Craig TA, Bowe AE, Vassiliadis J, Reczek D, Finnegan R, Jan De Beur SM, Schiavi SC, Kumar R. Secreted frizzled-related protein 4 is a potent tumor-derived phosphaturic agent. J. Clin. Invest 2003;112:785–794. [PubMed: 12952927]

Block GA, Port FK. Re-evaluation of risks associated with hyperphosphatemia and hyperparathyroidism in dialysis patients: recommendations for a change in management. Am. J. Kidney Dis 2000;35:1226–1237. [PubMed: 10845841]

Block GA, Hulbert-Shearon TE, Levin NW, Port FK. Association of serum phosphorus and calcium × phosphate product with mortality risk in chronic hemodialysis patients: a national study. Am. J. Kidney Dis 1998;31:607–617. [PubMed: 9531176]

Bowe AE, Finnegan R, Jan de Beur SM, Cho J, Levine MA, Kumar R, Schiavi SC. FGF-23 inhibits renal tubular phosphate transport and is a PHEX substrate. Biochem. Biophys. Res. Commun 2001;284:977–981. [PubMed: 11409890]

Bradley, A. Production and analysis of chimeric mice. In: Robertson, EJ., editor. Teratocarcinomas and Embryonic Stem Cells: A Practical Approach. IRL Press; Washington, DC: 1987. p. 113-152.

Campos M, Couture C, Hirata IY, Juliano MA, Loisel TP, Crine P, Juliano L, Boileau G, Carmona AK. Human recombinant PHEX has a strict S1′ specificity for acidic residues and cleaves peptides derived from FGF-23 and MEPE. Biochem. J 2003;373:271–279. [PubMed: 12678920]

Carpenter TO. Oncogenic osteomalacia—a complex dance of factors. N. Engl. J. Med 2003;348:1705–1708. [PubMed: 12711747]

Chertow GM, Burke SK, Lazarus JM, Stenzel KH, Wombolt D, Goldberg D, Bonventre JV, Slatopolsky E. Poly(allylamine hydrochloride) (RenaGel): a noncalcemic phosphate binder for the treatment of hyperphosphatemia in chronic renal failure. Am. J. Kidney Dis 1997;29:66–71. [PubMed: 9002531]

Collins AJ, Li S, Ma JZ, Herzog C. Cardiovascular disease in end-stage renal disease patients. Am. J. Kidney Dis 2001;38:S26–S29. [PubMed: 11576917]

De Beur SM, Finnegan RB, Vassiliadis J, Cook B, Barberio D, Estes S, Manavalan P, Petroziello J, Madden SL, Cho JY, et al. Tumors associated with oncogenic osteomalacia express genes important in bone and mineral metabolism. J. Bone Miner. Res 2002;17:1102–1110. [PubMed: 12054166]

Drezner, M. Phosphorus homeostasis and related disorders. In: Bilezikian, J.; Raisz, L.; Rodan, G., editors. Principles in Bone Biology. Academic Press; New York: 2002. p. 321-338.

Du L, Desbarats M, Viel J, Glorieux FH, Cawthorn C, Ecarot B. cDNA cloning of the murine Pex gene implicated in X-linked hypophosphatemia and evidence for expression in bone. Genomics 1996;36:22–28. [PubMed: 8812412]

Dunstan CR, Zhou H, Seibel MJ. Fibroblast growth factor 23: a phosphatonin regulating phosphate homeostasis? Endocrinology 2004;145:3084–3086. [PubMed: 15198971]

Econs MJ, McEnery PT, Lennon F, Speer MC. Autosomal dominant hypophosphatemic rickets is linked to chromosome 12p13. J. Clin. Invest 1997;100:2653–2657. [PubMed: 9389727]

Ganesh SK, Stack AG, Levin NW, Hulbert-Shearon T, Port FK. Association of elevated serum PO(4), Ca × PO(4) product, and parathyroid hormone with cardiac mortality risk in chronic hemodialysis patients. J. Am. Soc. Nephrol 2001;12:2131–2138. [PubMed: 11562412]

Holm IA, Huang X, Kunkel LM. Mutational analysis of the PEX gene in patients with X-linked hypophosphatemic rickets. Am. J. Hum. Genet 1997;60:790–797. [PubMed: 9106524]

HYP_Consortium. A gene (PEX) with homologies to endopeptidases is mutated in patients with X-linked hypophosphatemic rickets. Nat. Genet 1995;11:130–136. [PubMed: 7550339]

Imanishi Y, Inaba M, Nakatsuka K, Nagasue K, Okuno S, Yoshihara A, Miura M, Miyauchi A, Kobayashi K, Miki T, et al. FGF-23 in patients with end-stage renal disease on hemodialysis. Kidney Int 2004;65:1943–1946. [PubMed: 15086938]

Jonsson KB, Zahradnik R, Larsson T, White KE, Sugimoto T, Imanishi Y, Yamamoto T, Hampson G, Koshiyama H, Ljunggren O, et al. Fibroblast growth factor 23 in oncogenic osteomalacia and X-linked hypophosphatemia. N. Engl. J. Med 2003;348:1656–1663. [PubMed: 12711740]

Karaplis AC, Luz A, Glowacki J, Bronson RT, Tybulewicz VL, Kronenberg HM, Mulligan RC. Lethal skeletal dysplasia from targeted disruption of the parathyroid hormone-related peptide gene. Genes Dev 1994;8:277–289. [PubMed: 8314082]

Kronenberg HM. Developmental regulation of the growth plate. Nature 2003;423:332–336. [PubMed: 12748651]

Lanske B, Divieti P, Kovacs C, Pirro A, Landis W, Krane S, Bringhurst F, Kronenberg H. The parathyroid hormone/parathyroid hormone-related peptide receptor mediates actions of both ligands in murine bone. Endocrinology 1998;139:5194–5204. [PubMed: 9832460]

Larsson T, Nisbeth U, Ljunggren O, Juppner H, Jonsson KB, Riminucci M, Collins MT, Fedarko NS, Cherman N, Corsi A, et al. Circulating concentration of FGF-23 increases as renal function declines in patients with chronic kidney disease, but does not change in response to variation in phosphate intake in healthy volunteers. Kidney Int 2003;64:2272–2279. [PubMed: 14633152]

Larsson T, Marsell R, Schipani E, Ohlsson C, Ljunggren O, Tenenhouse HS, Juppner H, Jonsson KB. Transgenic mice expressing fibroblast growth factor 23 under the control of the {alpha}1(I) collagen promoter exhibit growth retardation, osteomalacia and disturbed phosphate homeostasis. Endocrinology 2004;145:3087–3094. [PubMed: 14988389]

Liu S, Guo R, Simpson LG, Xiao ZS, Burnham CE, Quarles LD. Regulation of fibroblastic growth factor 23 expression but not degradation by PHEX. J. Biol. Chem 2003;278:37419–37426. [PubMed: 12874285]

Lorenz-Depiereux B, Guido VE, Johnson KR, Zheng QY, Gagnon LH, Bauschatz JD, Davisson MT, Washburn LL, Donahue LR, Strom TM, Eicher EM. New intragenic deletions in the Phex gene clarify X-linked hypophosphatemia-related abnormalities in mice. Mamm. Genome 2004;15:151–161. [PubMed: 15029877]

McLeod MJ. Differential staining of cartilage and bone in whole fetuses by alcian blue and alizarin red S. Teratology 1980;22:299–301. [PubMed: 6165088]

Meric F, Yap P, Bia MJ. Etiology of hypercalcemia in hemodialysis patients on calcium carbonate therapy. Am. J. Kidney Dis 1990;16:459–464. [PubMed: 2239937]

Miao D, Bai X, Panda D, McKee M, Karaplis A, Goltzman D. Osteomalacia in hyp mice is associated with abnormal phex expression and with altered bone matrix protein expression and deposition. Endocrinology 2001;142:926–939. [PubMed: 11159866]

Nelson AE, Bligh RC, Mirams M, Gill A, Au A, Clarkson A, Juppner H, Ruff S, Stalley P, Scolyer RA, et al. Clinical case seminar: fibroblast growth factor 23: a new clinical marker for oncogenic osteomalacia. J. Clin. Endocrinol. Metab 2003;88:4088–4094. [PubMed: 12970268]

Ott SM, Maloney NA, Coburn JW, Alfrey AC, Sherrard DJ. The prevalence of bone aluminum deposition in renal osteodystrophy and its relation to the response to calcitriol therapy. N. Engl. J. Med 1982;307:709–713. [PubMed: 6896740]

Quarles LD. FGF23, PHEX, and MEPE regulation of phosphate homeostasis and skeletal mineralization. Am. J. Physiol: Endocrinol. Metab 2003;285:E1–E9. [PubMed: 12791601]

Riminucci M, Collins MT, Fedarko NS, Cherman N, Corsi A, White KE, Waguespack S, Gupta A, Hannon T, Econs MJ, et al. FGF-23 in fibrous dysplasia of bone and its relationship to renal phosphate wasting. J. Clin. Invest 2003;112:683–692. [PubMed: 12952917]

Rowe PS, Kumagai Y, Gutierrez G, Garrett IR, Blacher R, Rosen D, Cundy J, Navvab S, Chen D, Drezner MK, et al. MEPE has the properties of an osteoblastic phosphatonin and minhibin. Bone 2004;34:303–319. [PubMed: 14962809]

Saito H, Kusano K, Kinosaki M, Ito H, Hirata M, Segawa H, Miyamoto K, Fukushima N. Human fibroblast growth factor-23 mutants suppress Na+-dependent phosphate co-transport activity and 1alpha,25-dihydroxyvitamin D3 production. J. Biol. Chem 2003;278:2206–2211. [PubMed: 12419819]

Schenk, R.; Olah, A.; Herrmann, W. Preparation of calcified tissues for light microscopy. In: Dickson, G., editor. Methods of Calcified Tissue Preparation. Elsevier; Amsterdam: 1984. p. 1-56.

Schiavi SC, Kumar R. The phosphatonin pathway: new insights in phosphate homeostasis. Kidney Int 2004;65:1–14. [PubMed: 14675031]

Seufert J, Ebert K, Muller J, Eulert J, Hendrich C, Werner E, Schuuze N, Schulz G, Kenn W, Richtmann H, et al. Octreotide therapy for tumor-induced osteomalacia. N. Engl. J. Med 2001;345:1883–1888. [PubMed: 11756579]

Shimada T, Mizutani S, Muto T, Yoneya T, Hino R, Takeda S, Takeuchi Y, Fujita T, Fukumoto S, Yamashita T. Cloning and characterization of FGF23 as a causative factor of tumor-induced osteomalacia. Proc. Natl. Acad. Sci. U. S. A 2001;98:6500–6505. [PubMed: 11344269]

Shimada T, Muto T, Urakawa I, Yoneya T, Yamazaki Y, Okawa K, Takeuchi Y, Fujita T, Fukumoto S, Yamashita T. Mutant FGF-23 responsible for autosomal dominant hypophosphatemic rickets is resistant to proteolytic cleavage and causes hypophosphatemia in vivo. Endocrinology 2002;143:3179–3182. [PubMed: 12130585]

Shimada T, Kakitani M, Yamazaki Y, Hasegawa H, Takeuchi Y, Fujita T, Fukumoto S, Tomizuka K, Yamashita T. Targeted ablation of Fgf23 demonstrates an essential physiological role of FGF23 in phosphate and vitamin D metabolism. J. Clin. Invest 2004a;113:561–568. [PubMed: 14966565]

Shimada T, Urakawa I, Yamazaki Y, Hasegawa H, Hino R, Yoneya T, Takeuchi Y, Fujita T, Fukumoto S, Yamashita T. FGF-23 transgenic mice demonstrate hypophosphatemic rickets with reduced expression of sodium phosphate cotransporter type Iia. Biochem. Biophys. Res. Commun 2004b; 314:409–414. [PubMed: 14733920]

Slatopolsky E, Weerts C, Lopez-Hilker S, Norwood K, Zink M, Windus D, Delmez J. Calcium carbonate as a phosphate binder in patients with chronic renal failure undergoing dialysis. N. Engl. J. Med 1986;315:157–161. [PubMed: 3724805]

Slatopolsky EA, Burke SK, Dillon MA. RenaGel, a non-absorbed calcium- and aluminum-free phosphate binder, lowers serum phosphorus and parathyroid hormone. The RenaGel Study Group. Kidney Int 1999;55:299–307.

Strewler GJ. FGF23, hypophosphatemia, and rickets: has phosphatonin been found? Proc. Natl. Acad. Sci. U. S. A 2001;98:5945–5946. [PubMed: 11371627]

Strom T, Francis F, Lorenz B, Böddrich A, Econs M, Lehrach H, Meitinger T. Pex gene deletions in Gy and Hyp mice provide mouse models for X-linked hypophosphatemia. Hum. Mol. Genet 1997;6:165–171. [PubMed: 9063736]

Tenenhouse HS. X-linked hypophosphataemia: a homologous disorder in humans and mice. Nephrol. Dial. Transplant 1999;14:333–341. [PubMed: 10069185]

Weber TJ, Liu S, Indridason OS, Quarles LD. Serum FGF23 levels in normal and disordered phosphorus homeostasis. J. Bone Miner. Res 2003;18:1227–1234. [PubMed: 12854832]

White KE, Jonsson KB, Carn G, Hampson G, Spector TD, Mannstadt M, Lorenz-Depiereux B, Miyauchi A, Yang IM, Ljunggren O, et al. The autosomal dominant hypophosphatemic rickets (ADHR) gene is a secreted polypeptide overexpressed by tumors that cause phosphate wasting. J. Clin. Endocrinol. Metab 2001;86:497–500. [PubMed: 11157998]

White KE, Waguespack SG, Econs MJ. Case 29-2001: oncogenic hypophosphatemic osteomalacia. N. Engl. J. Med 2002;346:381–382. [PubMed: 11821524]

Xiao ZS, Crenshaw M, Guo R, Nesbitt T, Drezner MK, Quarles LD. Intrinsic mineralization defect in hyp mouse osteoblasts. Am. J. Physiol: Endocrinol. Metab 1998;38:E 700–E 708.

Yamashita T, Yoshioka M, Itoh N. Identification of a novel fibroblast growth factor, FGF-23, preferentially expressed in the ventrolateral thalamic nucleus of the brain. Biochem. Biophys. Res. Commun 2000;277:494–498. [PubMed: 11032749]

Yamazaki Y, Okazaki R, Shibata M, Hasegawa Y, Satoh K, Tajima T, Takeuchi Y, Fujita T, Nakahara K, Yamashita T, Fukumoto S. Increased circulatory level of biologically active full-length FGF-23 in patients with hypophosphatemic rickets/osteomalacia. J. Clin. Endocrinol. Metab 2002;87:4957–4960. [PubMed: 12414858]

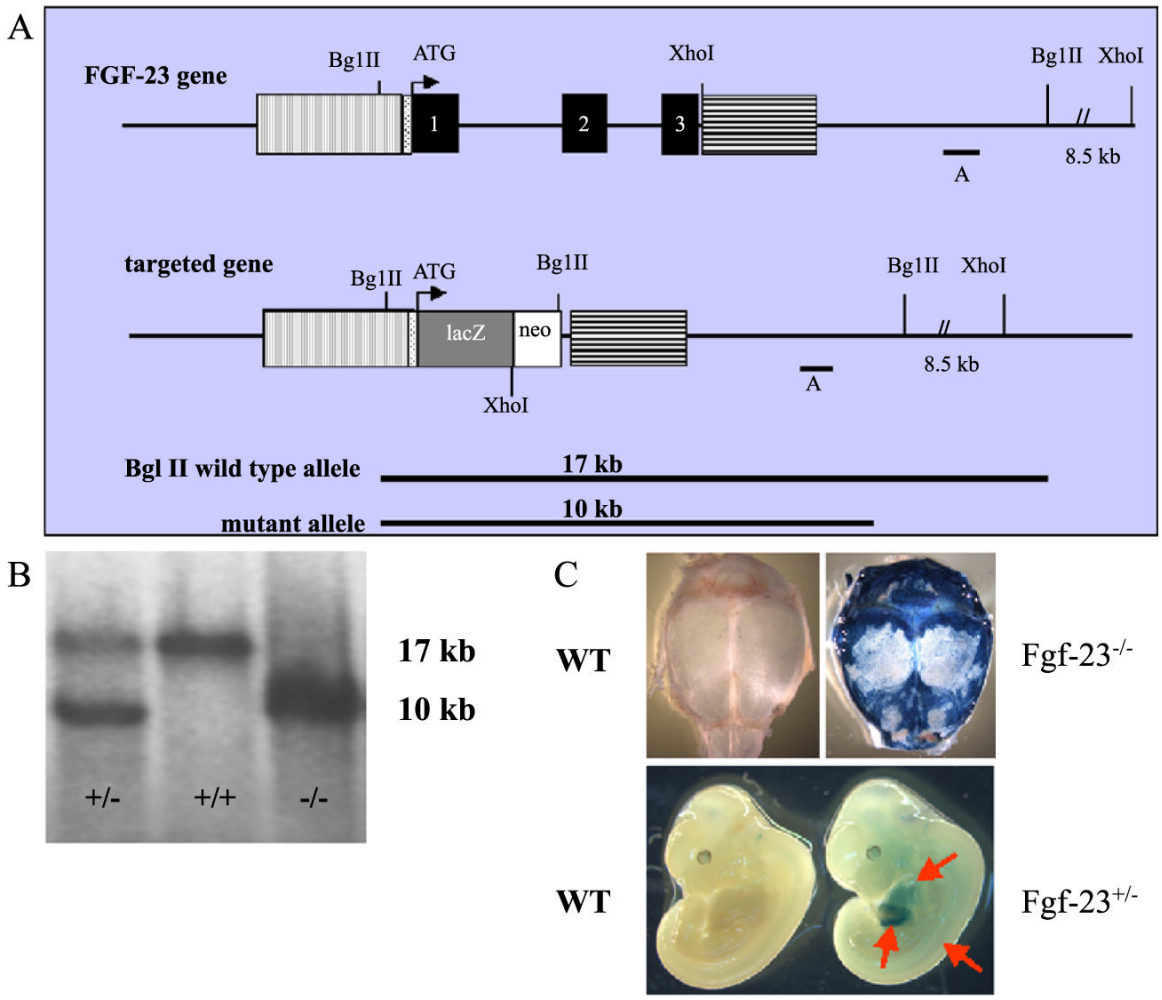

Fig. 1.

(A) Schematic representation of the murine *Fgf-23* gene and the corresponding knock-out/in targeting vector. Exons 1 to 3 are shown in black boxes. Vertical and horizontal shaded boxes represent the 5′ and 3′ flanking regions of the Fgf-23 gene, respectively, which were used for homologous recombination. The *lacZ* gene was cloned in frame with the initiator methionine of the *Fgf-23* gene. The *neomycin* resistance (neo) gene is driven by the phosphoglycerate kinase-1 (PGK-1) promoter and contains an Sv40 polyA adenylation site. Probe A was used as external probe to hybridize genomic Southern blots (*Bgl*II digest) shown in (B) (wild type= +/+, heterozygous=+/−, homozygous=−/−). Panel (C) represents lacZ staining of a wild-type (lower left) and a heterozygous *Fgf-23* embryo (*Fgf-23*$^{+/-}$, lower right) at E12.5. Arrows depict lacZ positive tissues (somites, liver, and heart). Upper panels demonstrate lacZ staining in a wild type (left) and *Fgf-23*$^{-/-}$ (right) skull at 3 weeks. Blue staining represents expression of the *Fgf-23* gene.

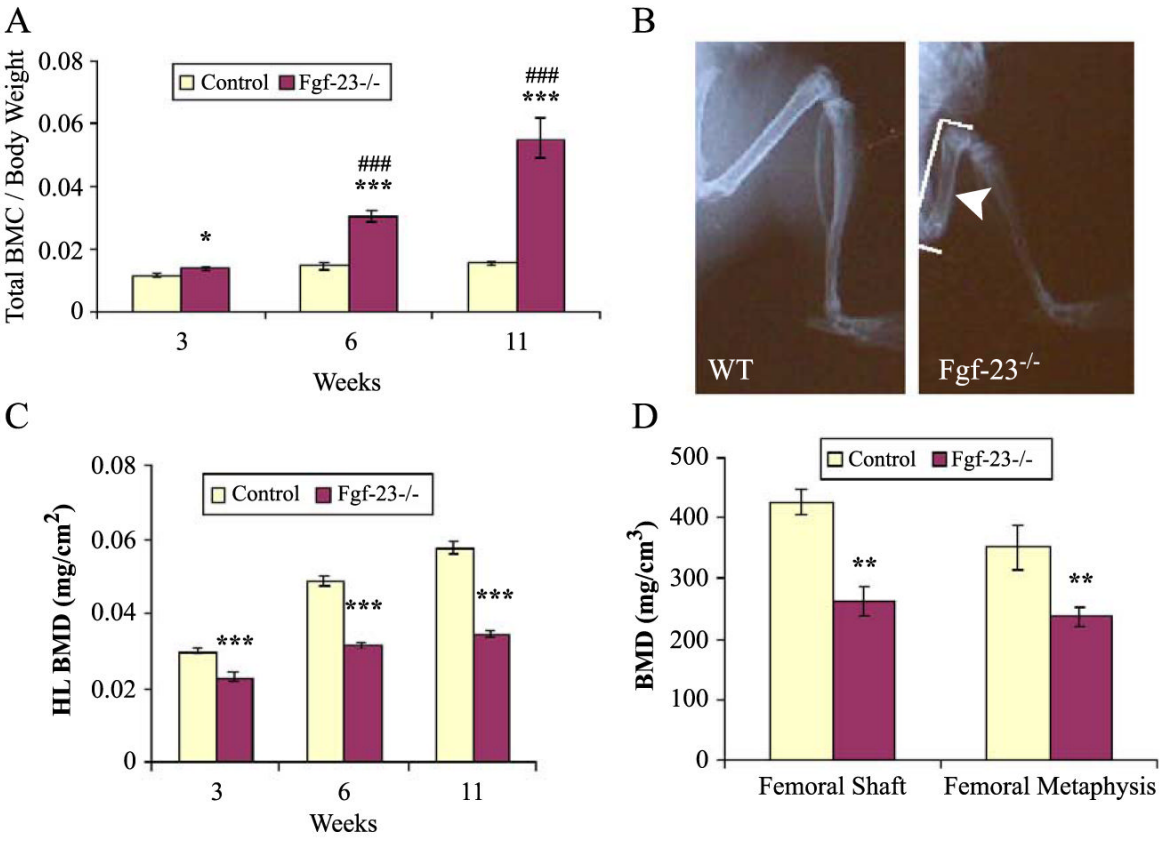

Fig. 2.

(A) Graphic display of total bone mineral content (BMC) of control and *Fgf-23*$^{-/-}$ animals at 3, 6, and 11 weeks. Each value obtained for BMC was normalized to the body weight of the corresponding animal. *Fgf-23*$^{-/-}$ mice show a statistical significant increase in total BMC when compared to control littermates (*=p<0.05; ***=p<0.0001). A statistically significant increase in total BMC was also observed among *Fgf-23*$^{-/-}$ mice with time (###=p<0.0001). (B) X-ray autoradiography of hindlimbs from a wild-type (WT) and an *Fgf-23*$^{-/-}$ mouse. Brackets depict length, and arrowhead depicts thickness of femur in *Fgf-23*$^{-/-}$ mouse. (C) Graph represents bone mineral density of hindlimbs measured by PIXImus analysis. *Fgf-23*$^{-/-}$ mice show a statistically significant decrease in BMD at 3, 6, and 11 weeks when compared to controls (***=p<0.0001). (D) BMD obtained from femoral shaft (left) and femoral methaphysis (right) of wild-type (white bar) and *Fgf-23*$^{-/-}$ animals (dark bar) by QCT at 4 weeks of age. *Fgf-23*$^{-/-}$ mice show a statistically significant decrease in BMD (**=p<0.001).

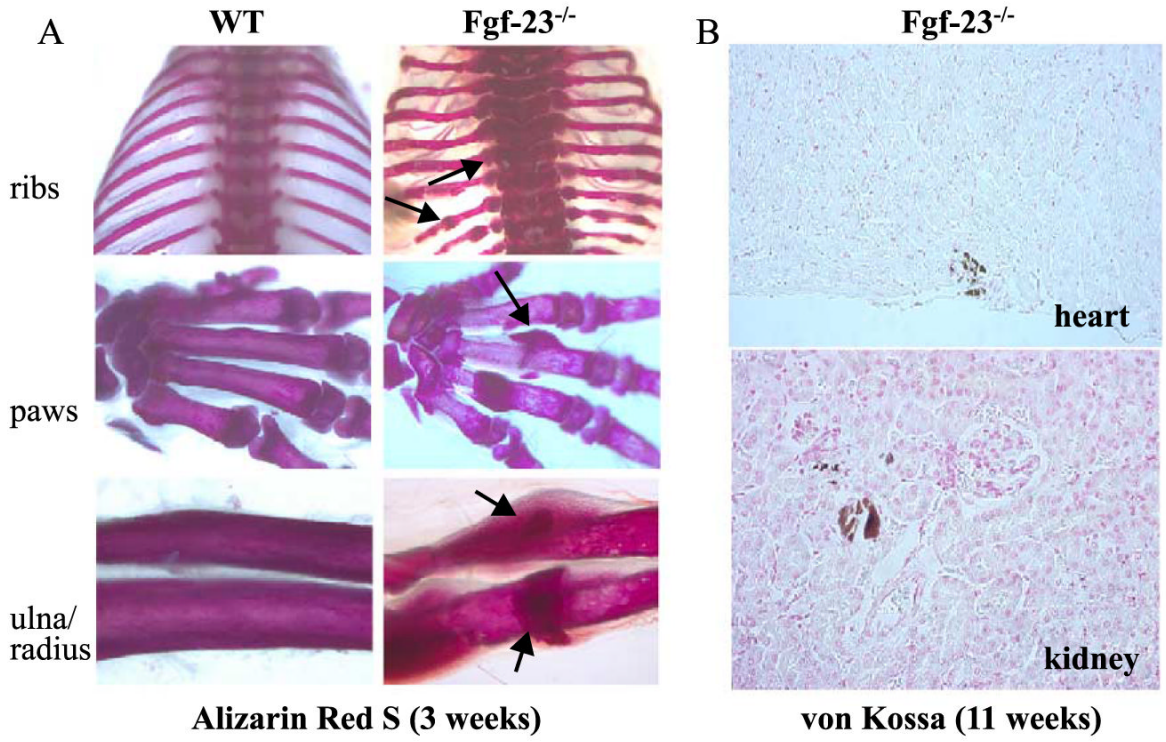

Fig. 3.

(A) Alizarin red S staining of skeletal elements (ribs, paws, ulna/radius) from a wild type (left panels) and *Fgf-23*$^{-/-}$ (right panels) at 3 weeks. Arrows depict some areas with abnormal mineralization in *Fgf-23*$^{-/-}$ bones. (B) Abnormal mineralization is shown in heart (top) and in and around the tubules of *Fgf-23*$^{-/-}$ kidney (bottom) at 11 weeks. (For interpretation of the references to colour in this figure legend, the reader is referred to the web version of this article.)

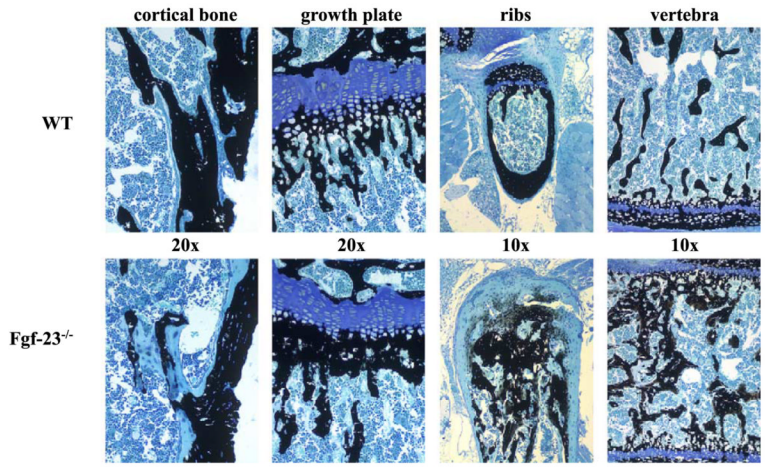

Fig. 4.

Three-micrometer-thick undecalcified sections from 4-week-old wild-type (upper panels) and *Fgf-23*$^{-/-}$ (lower panels) bones (cortical bone, growth plate, ribs, vertebra) were stained with von Kossa/McNeal (magnification 20×, 10×). Black staining represents mineralization. More mineral deposition is found in the area below the growth plate (methaphysis), ribs, and in vertebra. In contrast, areas of unmineralized osteoid (light blue) are found in cortical bone. (For interpretation of the references to colour in this figure legend, the reader is referred to the web version of this article.)

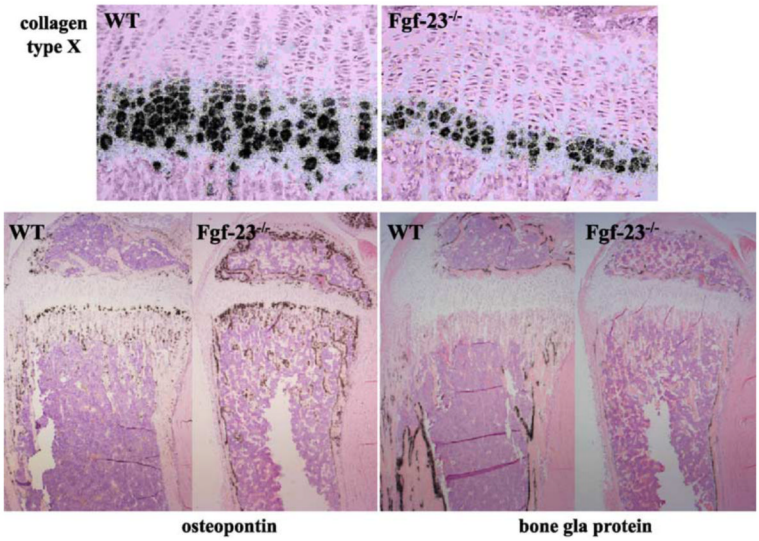

Fig. 5.

In situ hybridization was performed on 6μm-thick decalcified paraffin sections from tibia of wild-type (WT) and *Fgf-23*$^{-/-}$ animals at 3 weeks. The zone of hypertrophic chondrocytes was reduced in *Fgf-23*$^{-/-}$, which was confirmed by decreased collagen type X mRNA expression. In contrast, osteopontin mRNA expression was elevated in osteoblasts of *Fgf-23*$^{-/-}$ animals, while bone gla protein (osteocalcin) mRNA expression was diminished.

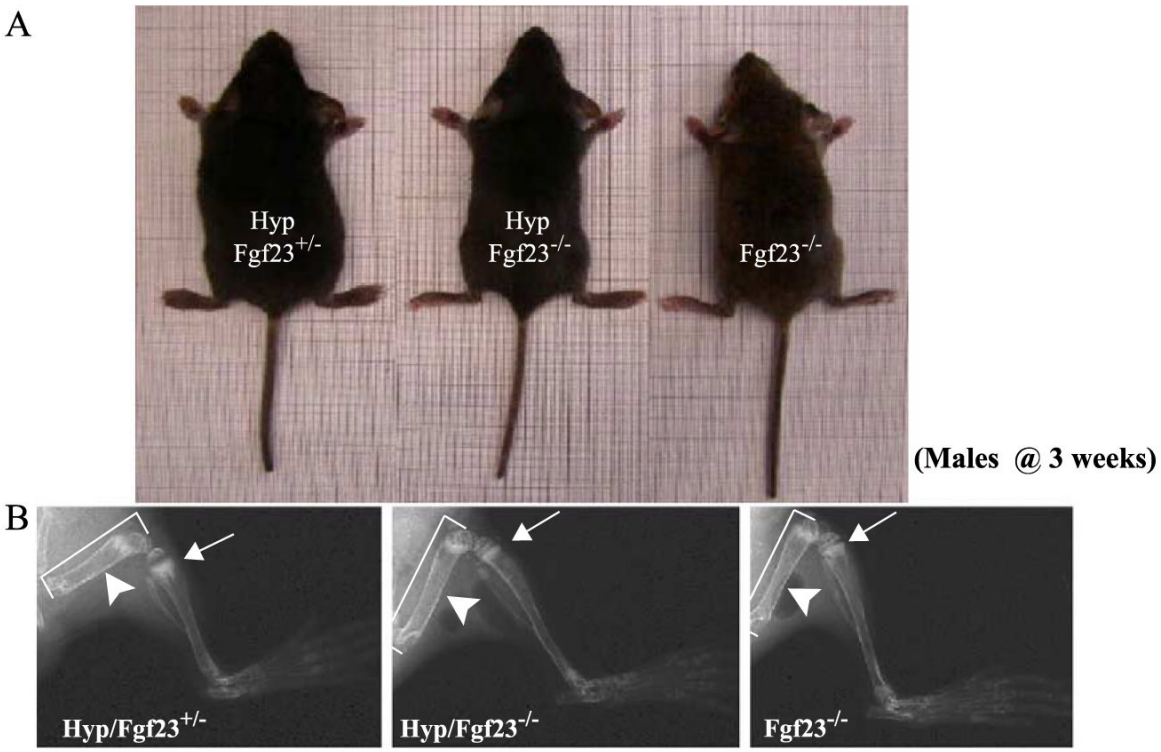

Fig. 6.

(A) Gross features of three male littermates at 3 weeks. Shown are *Hyp/Fgf23*$^{+/-}$ (left), *Fgf23*$^{-/-}$ (right), and compound mutants *Hyp/Fgf23*$^{-/-}$ (middle). (B) X-ray autoradiographs of hindlimbs from the same animals shown in panel (A). Arrows point to the growth plate of tibia. The features typical of rickets shown in *Hyp/Fgf23*$^{+/-}$ (left panel) had improved considerably in compound mutants *Hyp/Fgf23*$^{-/-}$ (middle panel). Arrowheads depict thickness of femoral shaft of these animals. *Hyp/Fgf23*$^{-/-}$ compound mutants (middle) exhibit longer (brackets) and thinner long bones than *Hyp/Fgf23*$^{+/-}$ (left) animals.

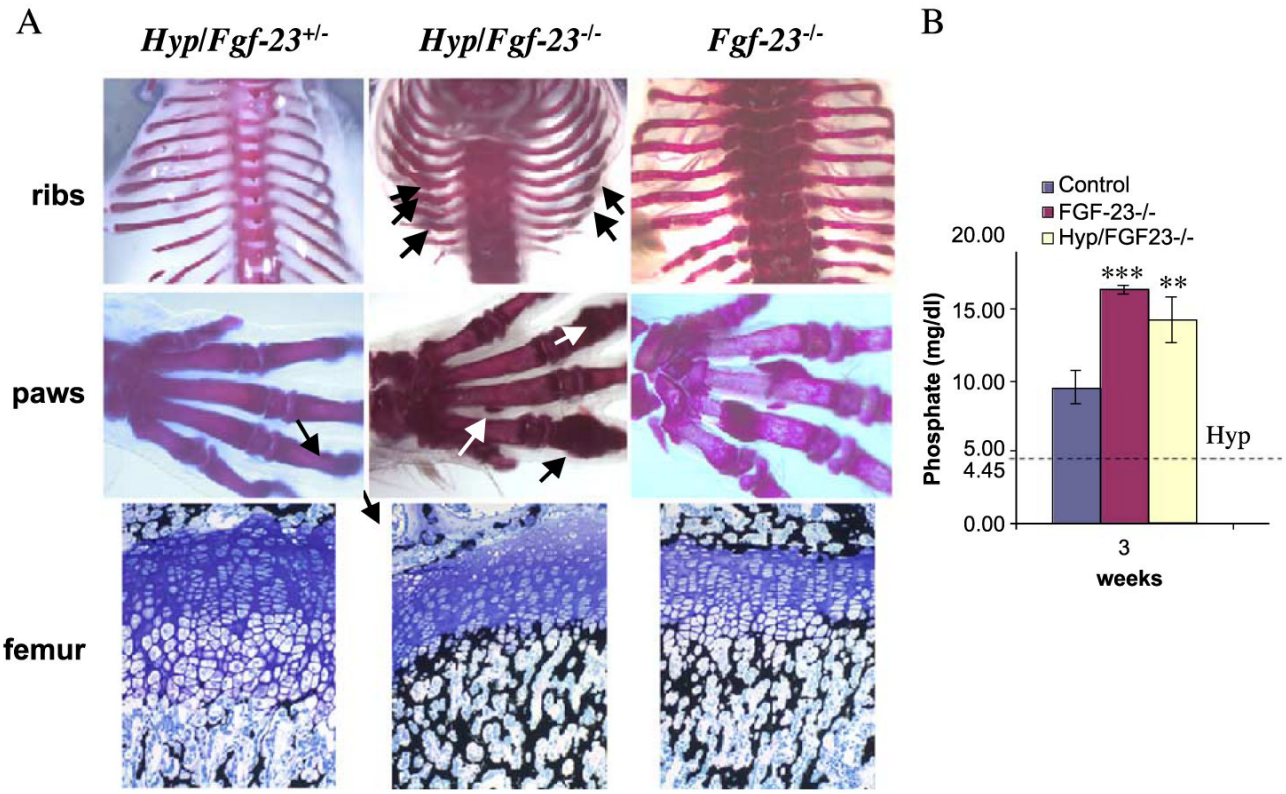

Fig. 7.

(A) Alizarin red S staining of skeletal elements (ribs, paws) from a *Hyp/Fgf23*$^{+/-}$ (left), *Hyp/Fgf23*$^{-/-}$ (middle), and *Fgf23*$^{-/-}$ (right) mice at 3 weeks. Arrows depict some areas with abnormal mineralization in *Hyp/Fgf23*$^{-/-}$ bones resembling the phenotype of *Fgf23*$^{-/-}$ skeleton. Lower panels represent 3μm-thick undecalcified sections from femur of 3-week-old *Hyp/Fgf23*$^{+/-}$ (left), *Hyp/Fgf23*$^{-/-}$ (middle), and *Fgf23*$^{-/-}$ (right) mice stained with Von Kossa/McNeal. Panel (B) represents a graph comparing serum phosphate levels of wild-type controls, *Fgf23*$^{-/-}$, and *Hyp/Fgf23*$^{-/-}$ compound mutants at 3 weeks of age. The horizontal dotted line illustrates published serum phosphate levels in *Hyp* mice (mean: 4.45 mg/dl) (***=p<0.0001; **=p<0.001) (Lorenz-Depiereux et al., 2004).